Supplement of Atmos. Meas. Tech., 19, 6973–6989, 2026
https://doi.org/10.5194/amt-19-6973-2026-supplement
© Author(s) 2026. CC BY 4.0 License.



Atmospheric Measurement Techniques
Open Access
EGU

Supplement of

Development and characterization of an advanced holographic instrument for atmospheric research

Susanne Glienke et al.

Correspondence to: Kevin L. Bertschinger (kevin.bertschinger@pnnl.gov) and Fan Mei (fan.mei@pnnl.gov)

The copyright of individual parts of the supplement might differ from the article licence.

Table S1. Specification of the prototype holographic system.

Instrument	Lens system	Wavelength (nm)	mode	pixel pitch (um)	sized	sample volume (cm^2)
HOLODROPS	lensless	355	pulse	3.45	6480x4860	106
HOLODROP-TRACK	lensless	532	CW	4.5	4096x2160	57
ePIV	Fixed focus	532	CW	4.86	1280x720	10

For HOLODROPS and HOLODROPS-TRACK to work effectively both systems need to be able to capture an intense image and have good holographic quality. Light attenuation and hologram quality are dependent on the particle size, particle density, and thickness which particles are being imaged. First Mie theory is used to estimated light attenuation that could be caused by using beer-lambert law. Then the shadow parameter is calculated to determine the expected hologram quality.

For inline holographic imaging, water particles are expected to attenuate the laser beam and cause multiple interferences. The attenuation effect of the particles can be analyzed using Mie theory, whereas the interference they produce will generate speckles in the inline imaging. To estimate holographic degradation caused by such interferences, Royer criteria can be employed (Royer, 1974; Tamrin and Rahmatullah, 2016)

Mie theory describes the scattering behavior of spherical particles when the particle size is comparable to the wavelength of light, making it a suitable model for analyzing the behavior of water droplets in this study. Assuming a distribution of water particles, their scattering coefficients can be calculated using the *miepython* package in Python. The size of water droplets can vary depending on environmental conditions, and their interaction with laser beams also depends on the droplet size. For this experiment, a 405 nm laser is used to illuminate the particles, making scattering within this wavelength range the primary focus.

Mie theory is particularly suitable for scenarios where the wavelength of light is comparable to the size of the particles causing scattering. In this experiment, the 405 nm laser wavelength, coupled with water particles having a minimum diameter of 5 μm, results in a relatively constant scattering efficiency as shown in Figure S1. Additionally, water droplets are well-known for exhibiting strong forward scattering behavior.

The scattering, absorption, and extinction coefficients can be determined using the following equations:

$$\epsilon_{sc} = N\left(\frac{\pi D^2}{4}\right)Q_{sc} \tag{1}$$

$$\epsilon_{abs} = N\left(\frac{\pi D^2}{4}\right)Q_{abs} \tag{2}$$

$$\epsilon_{ext} = N\left(\frac{\pi D^2}{4}\right)Q_{ext} \tag{3}$$

Here, N represents the number concentration of particles ((particles/cm^3)), D is the particle diameter, and Q_x denotes the efficiency factors for scattering Q_{sc}, absorption Q_{abs}, and extinction Q_{ext}. The efficiency factors Q_x can be calculated for each particle in the distribution using the *miepython* package in Python at a wavelength of 405 nm .

To determine inline attenuation, the Beer-Lambert law is applied, assuming the single scattering approximation ((Noaa), 2008). Using the extinction coefficient, the attenuation of laser light intensity is calculated as:

$$I(z) = I_0 e^{-\epsilon_{ext} z} \tag{4}$$

The attenuation behavior was modeled for various particle concentrations and propagation distances. The results are illustrated in Figure S1. Two different particle distribution are considered. The first case assumes the mean particle distribution is close to the wavelength of the laser light at $0.5\ \mu m$. Then in the second case, with a mean $15\ \mu m$ which is consistent with the size of fog (Podzimek, 1997; Nelli et al., 2024). For an extreme case of 5000 particles per cubic centimeter ((particles/cm^3)), laser light remains visible over a distance of up to 500 cm. This demonstrates the suitability of inline holographic imaging for environments with high particle densities.

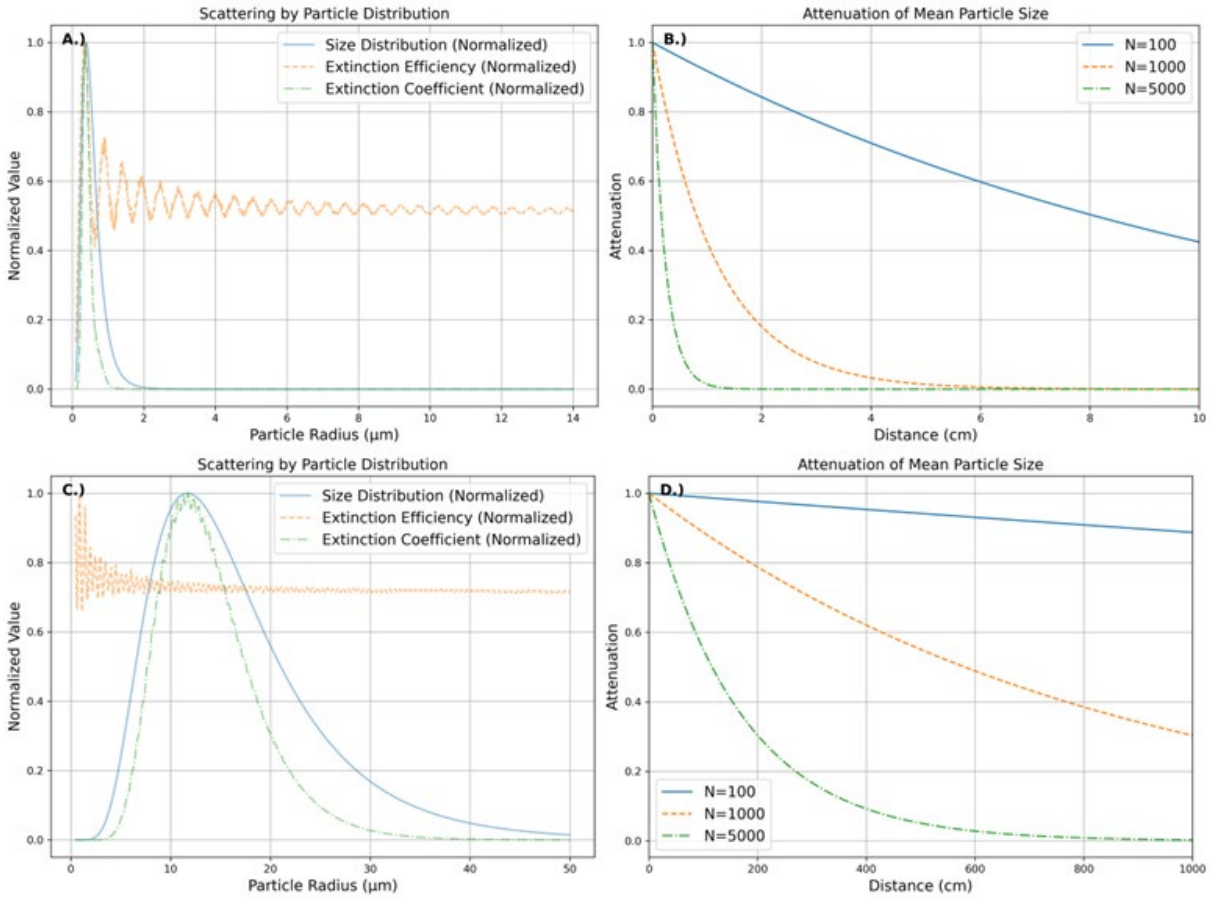


Figure S1: A.) A particle size distribution with the mean value is close to the wavelength of light at 05 μm. B.) attenuation of light for different number concentration of water droplets(number/um^3) over 10 cm for a particle distribution in panel A.). C.) A particle distribution with a mean size of 15 μm which is consistent with the size of fog. D) attenuation of light for different number concentration of water droplets(number/um^3) over 1000 cm for a particle distribution in panel D.).

In inline holography, the presence of water droplets acts as individual scatterers, contributing to speckle noise in the captured hologram. The quality of the hologram after passing through a distribution of particles can be characterized by the shadow density parameter, also known as the Royer criterion, given by the equation:

$$S = N(\pi D_{mean}^2)Z \tag{5}$$

Here, N represents the particle concentration ((particles/cm^3)), D_{mean} is the mean particle diameter, and Z is the propagation distance (Meng et al., 1993).

As described in Meng et al. (Meng et al., 1993), the value of the shadow density parameter determines the quality of the resulting hologram:

- (S < 0.01): High-quality hologram.
- (0.01 <S ≤ 0.1): Marginal hologram.
- (S > 0.1): Poor-quality hologram.

The calculated results of the shadow density parameters for various experimental configurations are presented in Figure S2, demonstrating the relationship between particle concentration, mean particle size, and imaging distance on hologram quality.

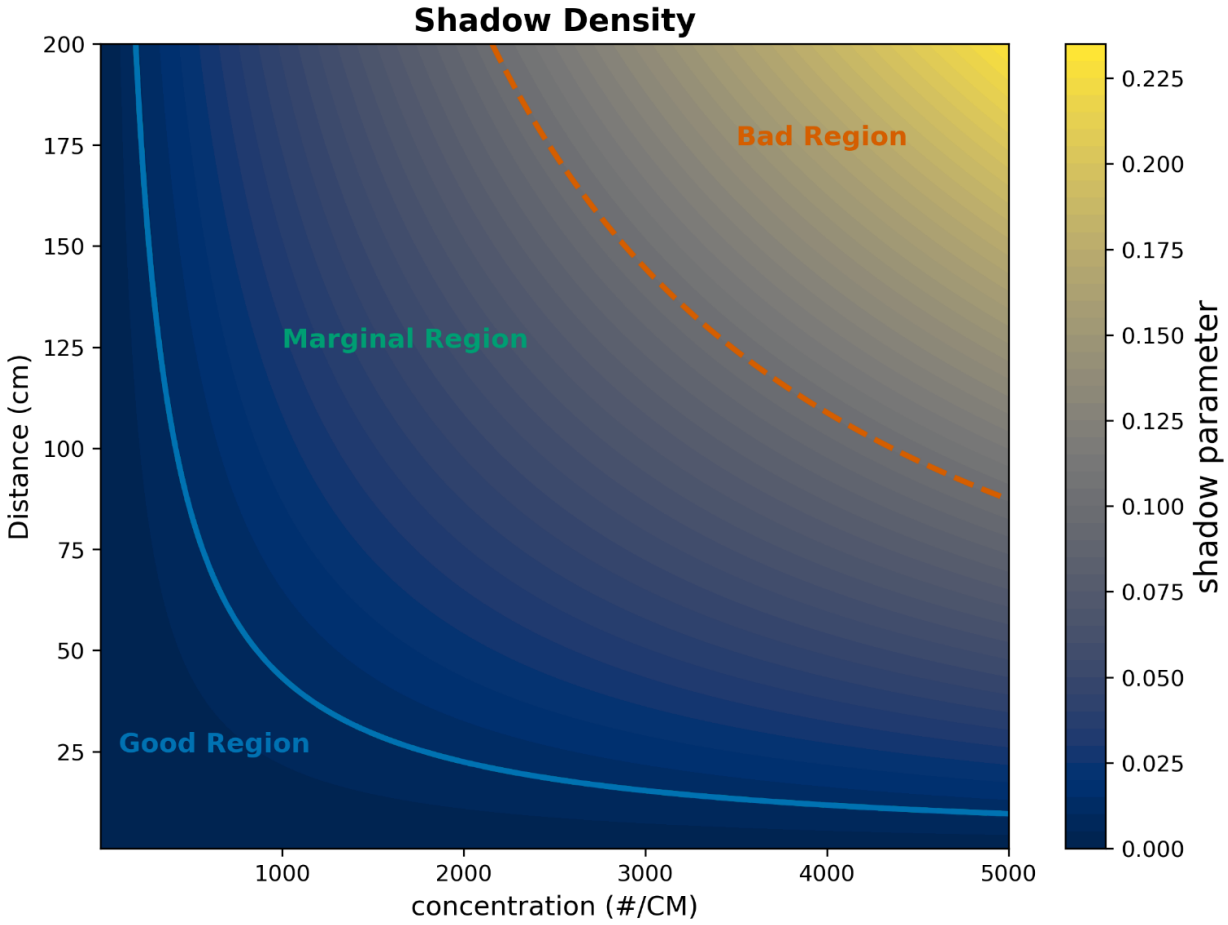


Figure S2 shadow parameters for holographic quality in terms of concentration and distance. The good, marginal and bad regions are separated by a line defining the respected value.

In conclusion, particle scattering is expected to have little effect on the light attenuation since the particle size with the most effective particle size is well below the resolution limit of the system. In addition, both systems should be able to collect holograms with particle densities of less than 1000/cm^3 and up to 1 meter optical depth.

To capture the varying turbulence flows the openPIV method outline in 2.2 ePIV prototype was ran for different time intervals. The laboratory had a steady breeze that would cause particles to steadily flow in the -x plane in the ePIV field of view. To draw a fair comparison the time duration was capture consistently at over 10 seconds total. The effect of keeping the time interval shorter shows more varied and turbulent flows throughout the measurements. This also results in more steady mean flows as shown in Figure S3 which shows the velocity fields for 1.0 ms, 5.0 ms, 10.0 ms, and 15.0 ms time intervals for the analysis process. As the time intervals decrease the mean flow fields show strong flow lines from in the negative x direction. In addition, as the time intervals increases, the average mean values gradually decreases, and flow fields become more varied.

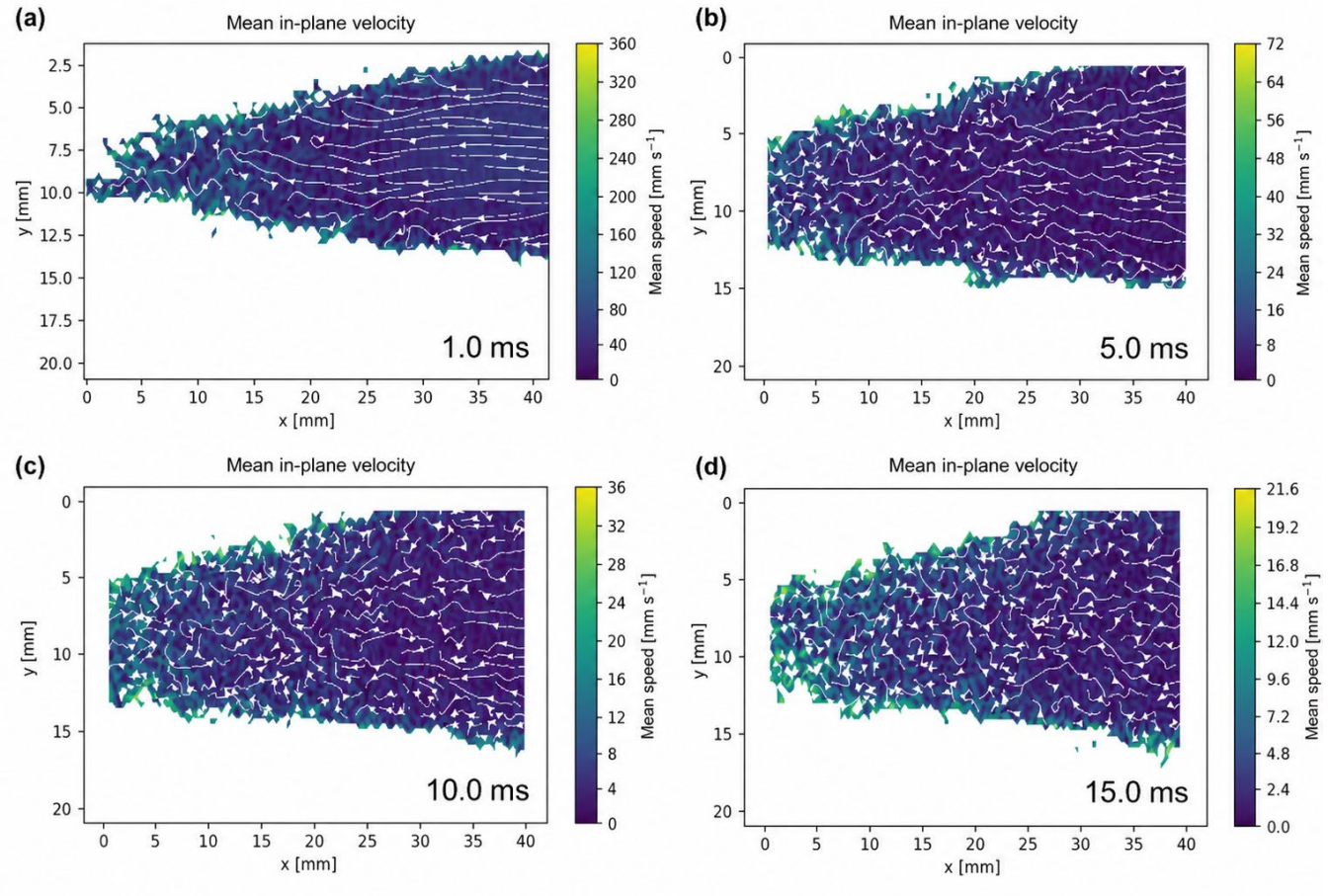


Figure S3: The following plot shows the time average velocity fields for different time intervals with the overall acquisition period kept longer than 10 seconds. A.) is for 1.0 ms, B.) is for 5.0 ms, C.) is for 10.0 ms, and (d) is for 15.0 ms. As the time interval increases more turbulent flows become present leading to a higher magnitude in velocity. Subsequently, the average value becomes more consistent in one direction as indicated by the streamlines.

Figure S4 shows the mean velocity per frame, and the cumulative mean over the duration of the measurement. As the time interval is increased the flow fields converge to a steady value faster. In addition, the mean field decreases as the time interval increases. This is attributed to longer intervals not capturing the turbulent dynamics that are present as the particles transverse in the -x direction of the cameras field of view. There is also not a continuous flow present in every frame which is captured by gaps in the data.

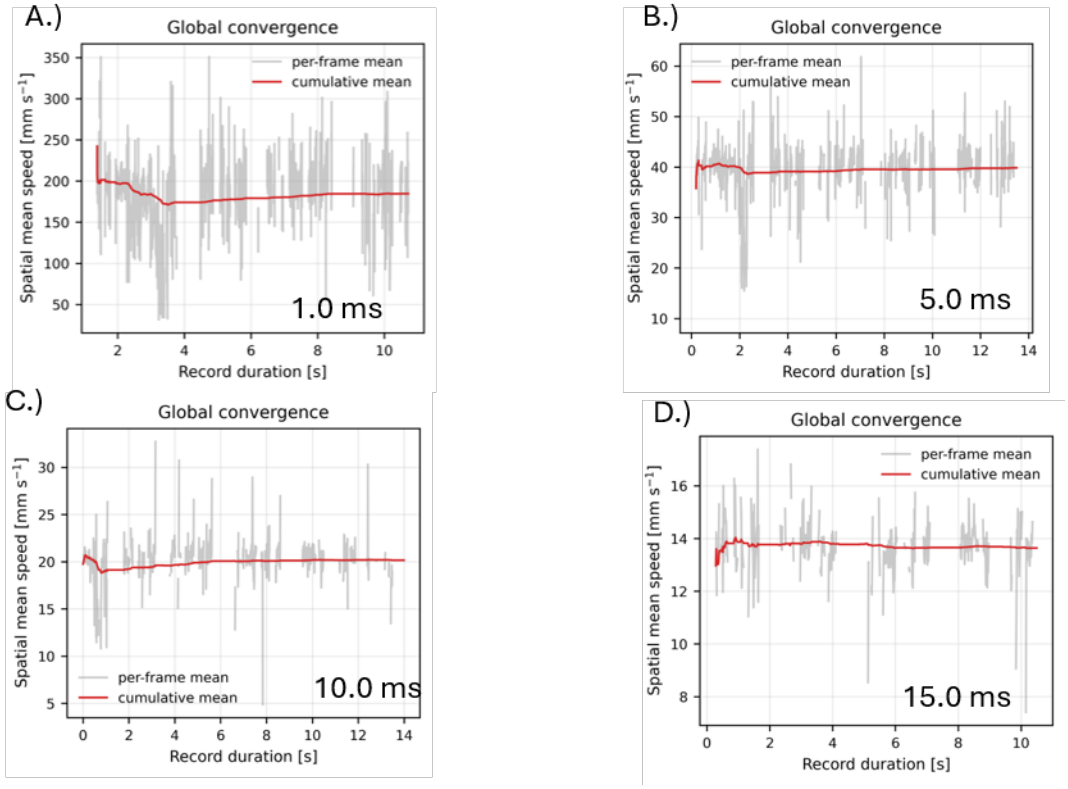


Figure S4 Shows the instantaneous velocity and convergence of the continuous mean values for different pseudo frame time intervals. A.) 1.0 ms, B.) 5.0 ms, C._)10.0 ms, and D.) 15.0 ms.

To better capture the turbulence nature of the fluid flow, Reynolds decomposition was applied. Reynolds decomposition separates each instantaneous velocity component into a mean and a fluctuating part, $u_i(x,t) = \bar{u_i}(x) + u_i'(x,t)$, where the overbar denotes a time average and the primed term captures the turbulent fluctuation about that mean. Applying this decomposition to the velocity field measured at each point allows the second-order statistics of the flow to be isolated from the mean advection. The covariance of the fluctuating velocity components, $\overline{u_i'u_j'}$, forms the Reynolds stress tensor and quantifies the degree to which fluctuations in different directions are correlated rather than independent. The diagonal terms ($\overline{u'^2}$, $\overline{v'^2}$) give the variance of the streamwise and wall-normal fluctuations and are directly related to the turbulent kinetic energy, while the off-diagonal term ($\overline{u'v'}$), the Reynolds shear stress, indicates the extent to which momentum is transported across the flow by turbulent motion; a nonzero value reflects a systematic correlation between streamwise and wall-normal fluctuations, as occurs when coherent turbulent structures sweep higher-momentum fluid toward the wall or ejected lower-momentum fluid away from it (Beresh et al., 2018). For the measured particle flows, it is observed that the covariance field are more prominent towards the end of the flow, then when exiting the nozzle.

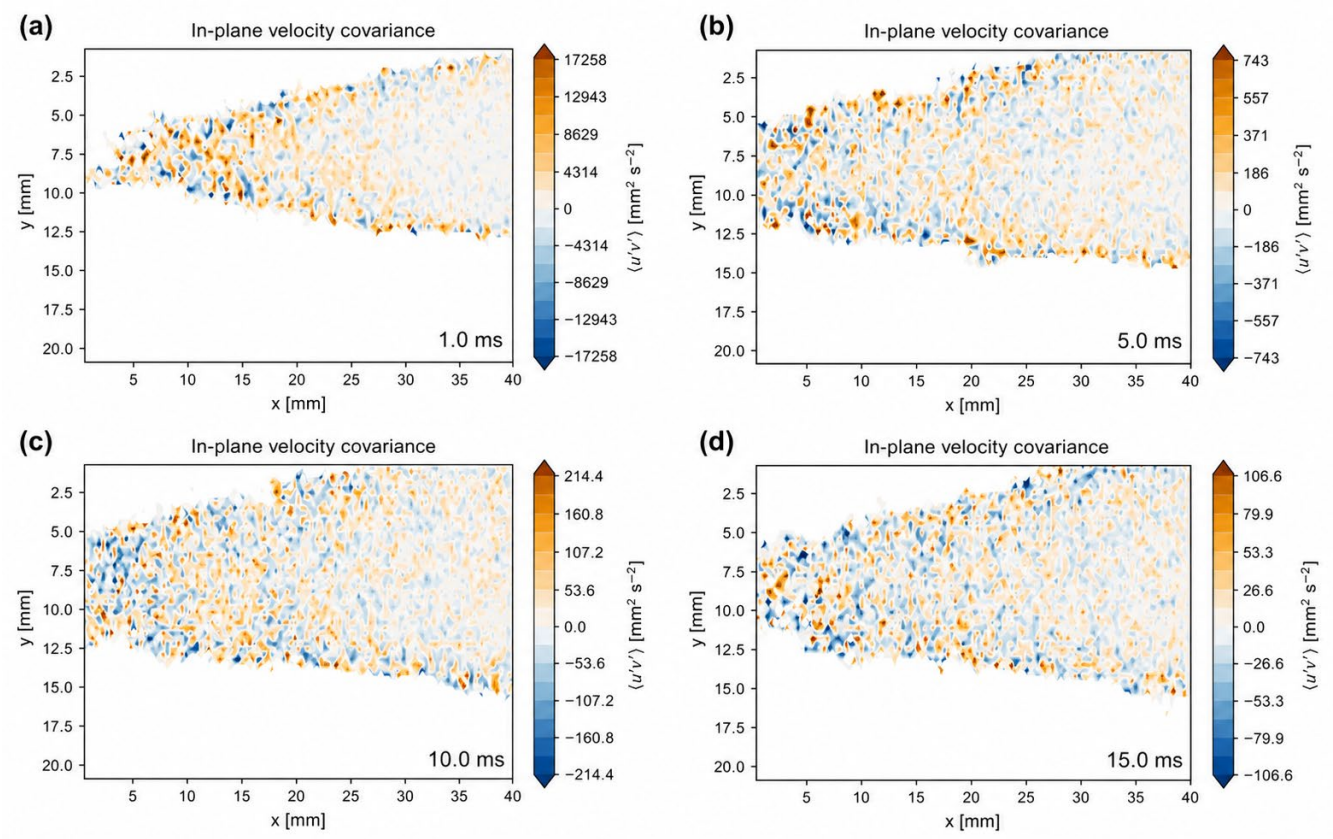


Figure S5 The following plots hows the velocity covariance from different time intervals. A.) is for 1.0 ms, B.) is for 5.0 ms, C.) is for 10.0 ms, and (d) is for 15.0 ms. As the time intervals increases the covariance across the flow decreases since the velocity fields become less apparent for longer time intervaa